Supplementary Information

Janus metal enabled tunable Schottky barriers in van der Waals contacts via interfacial polarization modulations

Yanze Feng[a,b], Liujian Qi*[a,b], Yu Du[a,b], Nan Zhang[a,b], Yuting Zou[a,b], Zhiming Shi[a,b], Dabing Li[a,b], Shaojuan Li*[a,b]

[a]State Key Laboratory of Luminescence Science and Technology, Changchun Institute of Optics, Fine Mechanics and Physics, Chinese Academy of Sciences, Changchun 130033, China.

[b]University of Chinese Academy of Sciences (UCAS), Beijing 100049, China.

*Email: qiliujian@ciomp.ac.cn; lishaojuan@ciomp.ac.cn

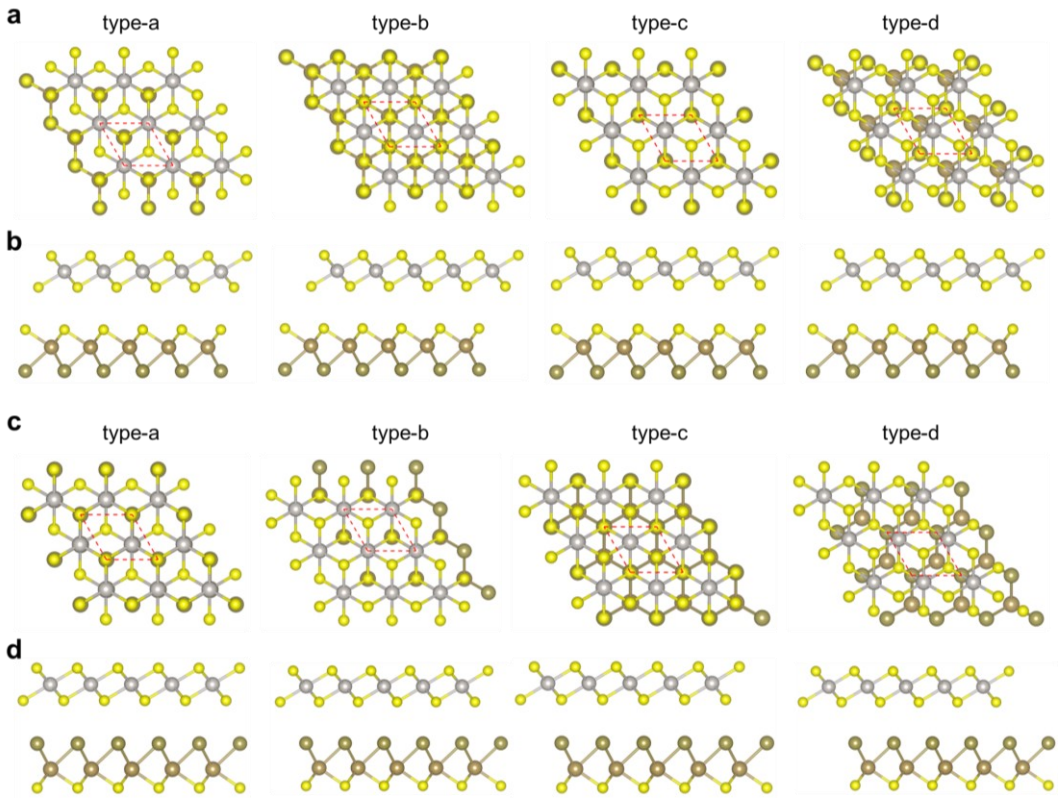

Fig. S1 Top and side views of the different stacking configurations of PtS_2-STaTe (a, b) and PtS_2-TeTaS (c, d) heterostructures, respectively.

Table S1 Total energy (eV) of different possible stacking configurations for PtS_2 and Janus metal contacts.

Energy (eV)	Interface	Type-a	Type-b	Type-c	Type-d
PtS_2-TaSTe	S	-37.9215	-37.9187	-37.8288	-37.9187
	Te	-37.9113	-37.9117	-37.8182	-37.9111
MoS_2-TaSTe	S	-154.5506	-154.5442	-154.4862	---
	Te	-154.5182	-154.4543	-154.4509	---
PtS_2-NbSTe	S	-36.5467	-36.4916	-36.4358	-36.4896
	Te	-36.5039	-36.5229	-36.4044	-36.5227
PtS_2-TaPTe	P	-38.2578	-38.1205	-38.1129	-38.1285
	Te	-38.1133	-38.1118	-38.0211	-38.1114
PtS_2-CrSTe	S	-34.7192	-34.8102	-34.8122	-34.8100
	Te	-34.6914	-34.7803	-34.7708	-34.7812
PtS_2-TiSTe	S	-34.7855	-34.8816	-34.8458	-34.8457
	Te	-34.8606	-34.8681	-34.7806	-34.8603
PtS_2-ZrSTe	S	-35.9473	-35.9095	-35.8520	-35.9089
	Te	-35.9462	-35.9289	-35.8470	-35.9289
PtS_2-HfSTe	S	-37.3412	-37.3096	-37.2481	-37.3091
	Te	-37.3483	-37.3317	-37.2495	-37.3312

Table S2 Binding energy (eV), interface distance (Å) and lattice mismatch of the most stable stacking configurations for PtS_2 and Janus metal contacts.

Type	Interface	E_b (J/m^2)	*d* (Å)	Mismatch
PtS_2-TaSTe	S	-0.44	2.85	1.70%
	Te	-0.43	3.05	
MoS_2-TaSTe	S	-0.38	3.18	4.20%
	Te	-0.36	3.49	
PtS_2-NbSTe	S	-0.49	2.64	1.70%
	Te	-0.45	2.97	
PtS_2-TaPTe	P	-0.64	2.44	0.56%
	Te	-0.43	2.98	
PtS_2-CrSTe	S	-0.46	2.81	3.43%
	Te	-0.41	3.07	
PtS_2-TiSTe	S	-0.43	2.79	0.28%
	Te	-0.41	3.08	
PtS_2-ZrSTe	S	-0.44	2.77	7.05%
	Te	-0.44	2.92	
PtS_2-HfSTe	S	-0.43	2.81	5.99%
	Te	-0.44	2.96	

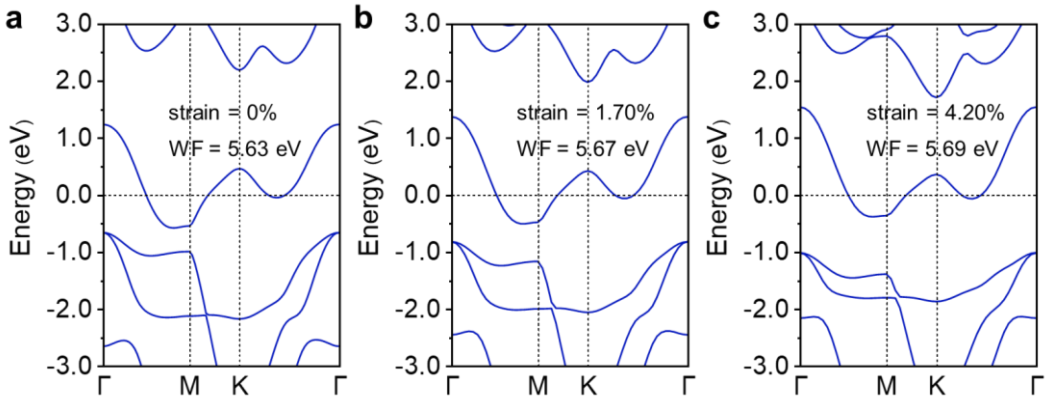

Fig. S2 Band structures of monolayer PtS_2 under the strain of (a) 0%, (b) 1.70% and (c) 4.20%. WF represents the work function.

Table S3 The SBHs of PtS_2-ZrSTe and PtS_2-HfSTe systems under different strain calculated by the GGA-PBE functional due to large periodic cells with 159 atoms for the smaller lattice mismatch.

(eV)	PtS_2-SZrTe		PtS_2-TeZrS		PtS_2-SHfTe		PtS_2-TeHfS	
strain	7.05%	1.37%	7.05%	1.37%	5.99%	0.32%	5.99%	0.32%
Φ_{SB}-n	0.49	0.35	0.22	0.32	0.24	0.22	0.11	0.23
Φ_{SB}-n	1.28	1.23	1.12	1.01	1.41	1.39	1.23	1.14

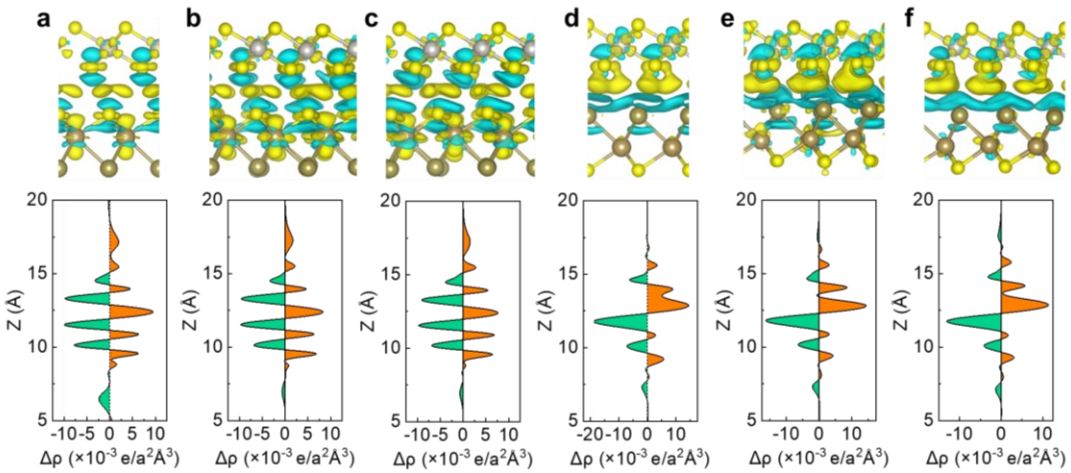

Fig. S3 Three-dimensional and plane charge density differences of PtS_2-STaTe (a-c) and PtS_2-TeTaS (d-f) heterostructures under 0 K (a and d) and 300 K (b, c; e, f, randomly sampled snapshots) lattice vibrations and thermal fluctuations, respectively. Here, the unit $\Delta\rho$ of is unified as $e/a^2Å^3$ for comparison, a is the lattice constant of unit cell. The isosurface of charge density differences is 1.8×10^{-4} e $bohr^{-3}$.

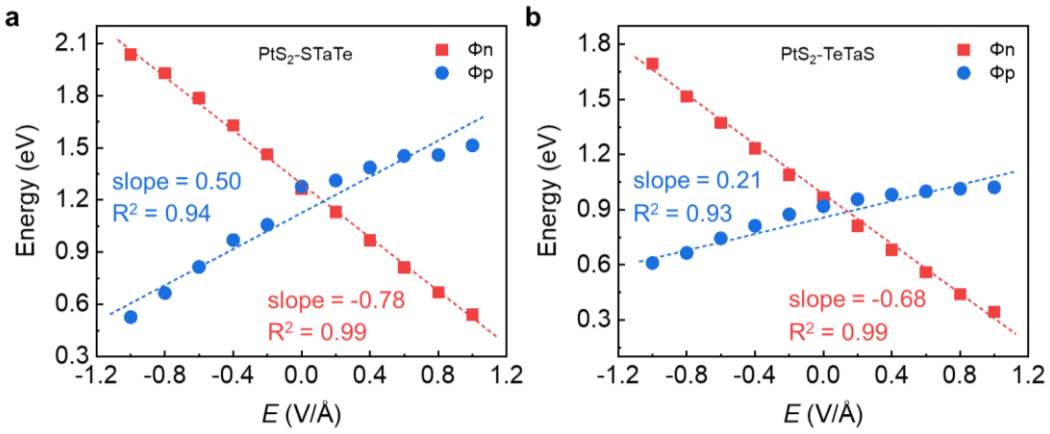

Fig. S4 Evolutions of *n*- and *p*-type SBHs under different external electric fields for (a) vdW PtS_2-STaTe and (b) vdW PtS_2-TeTaS heterostructures, respectively.

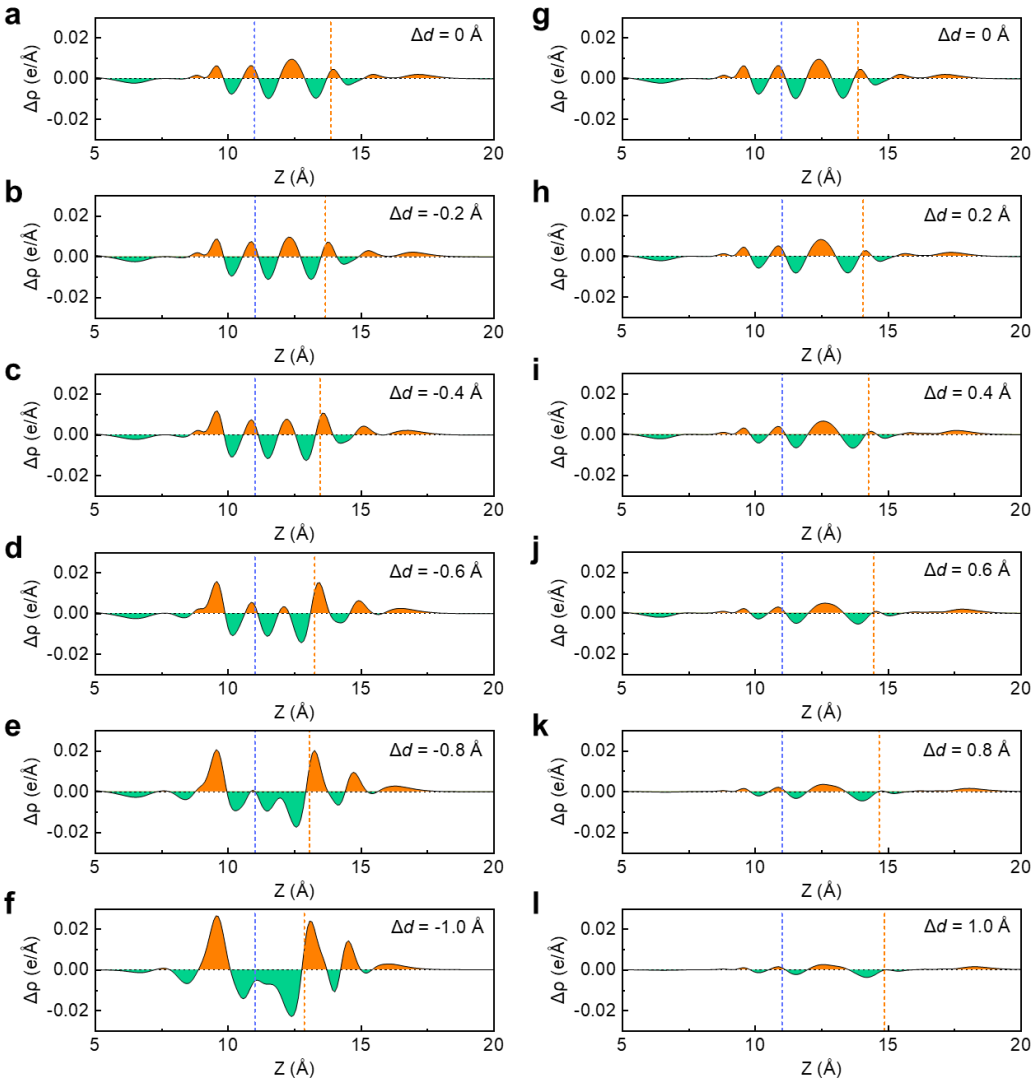

Fig. S5 Evolutions of plane charge density differences under different compression (a)-(f) and (g)-(l) tension strains for vdW PtS_2-STaTe heterostructures. The z-coordinates in these figures are manually aligned with the atom z-coordinate of Janus TaSTe for comparative purposes. The vertical dashed lines are associated to the center of mass of each 2D material, the orange and blue dashed lines correspond to PtS_2 and Janus TaSTe, respectively.

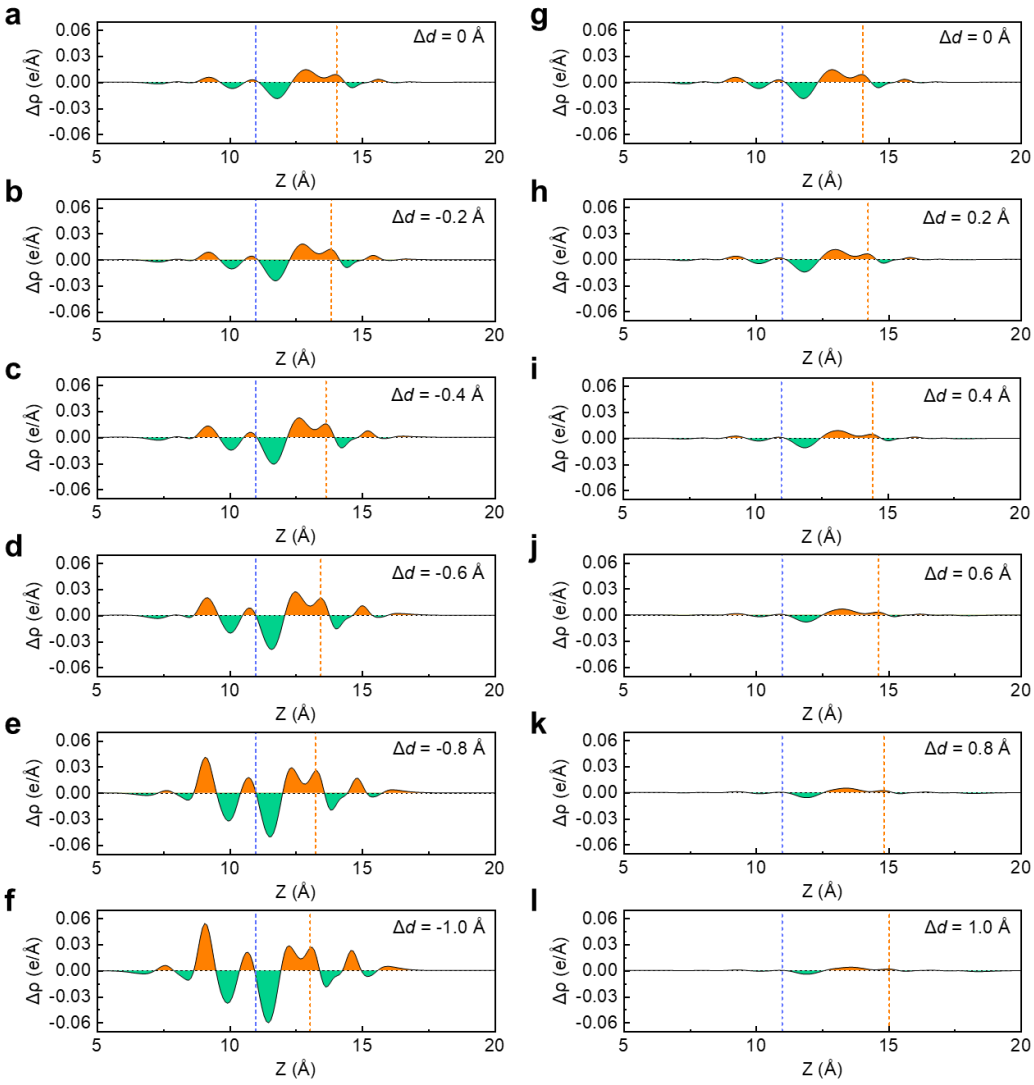

Fig. S6 Evolutions of plane charge density differences under different compression (a)-(f) and (g)-(l) tension strains for vdW PtS_2-TeTaS heterostructures. The z-coordinates in these figures are manually aligned with the atom z-coordinate of Janus TaSTe for comparative purposes. The vertical dashed lines are associated to the center of mass of each 2D material, the orange and blue dashed lines correspond to PtS_2 and Janus TaSTe, respectively.

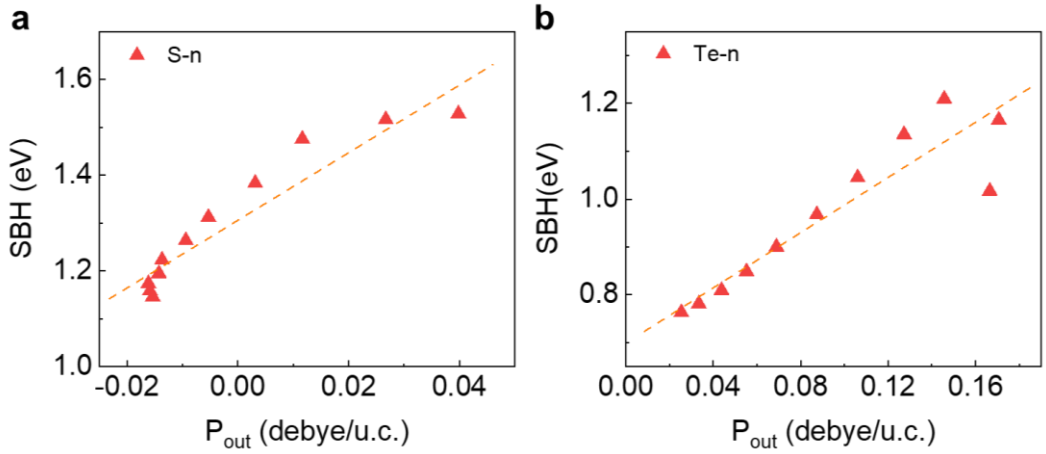

Fig. S7 Evolutions of n-type SBH versus the out of-plane interfacial polarizations for vdW PtS_2-STaTe and PtS_2-TeTaS heterostructures, respectively. The dashed lines indicate the variation trend of SBH versus interfacial polarization.

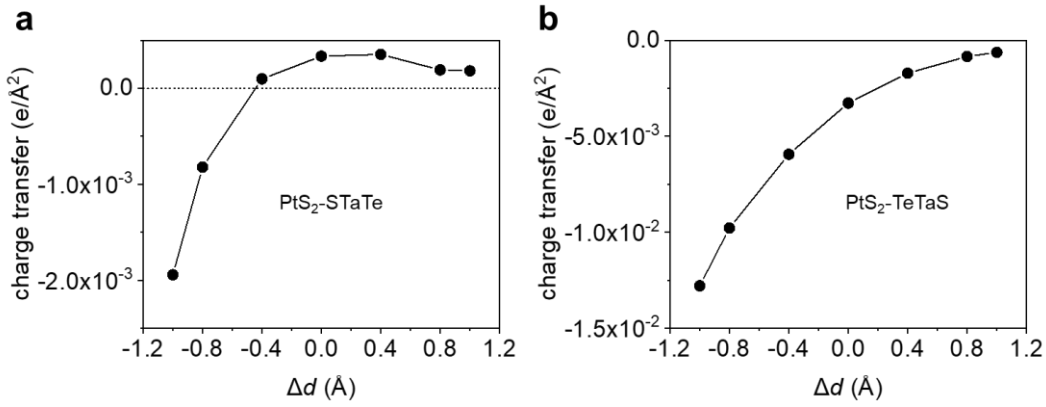

Fig. S8 Charge transfer between TaSTe and PtS_2 in PtS_2-STaTe (a) and PtS_2-TeTaS (b) heterostructures, respectively. Here, the negative value represents the charge transfer form TaSTe to PtS_2.

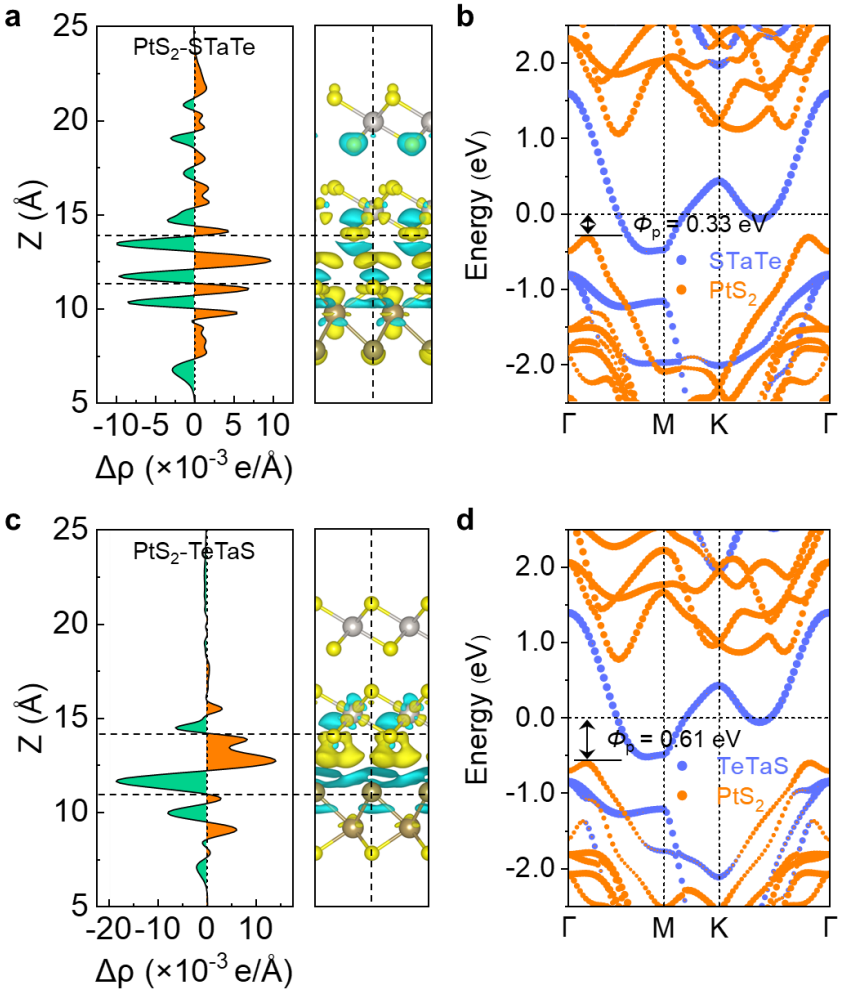

Fig. S9 (a) and (c) Plane and three-dimensional charge density differences, (b) and (d) Projected band structures of vdW 2L PtS_2-STaTe and 2L PtS_2-TeTaS heterostructures, respectively. Orange and blue colors in band structures represent the contributions from PtS_2 and TaSTe, respectively. In both (a) and (c), the isosurface of charge density differences is 1.8×10^{-4} e $bohr^{-3}$, and the yellow and cyan regions of three-dimensional charge density differences represent the electron accumulation and depletion, respectively. The orange and blue colors in band structures represent the contributions from PtS_2 and TaSTe, respectively.

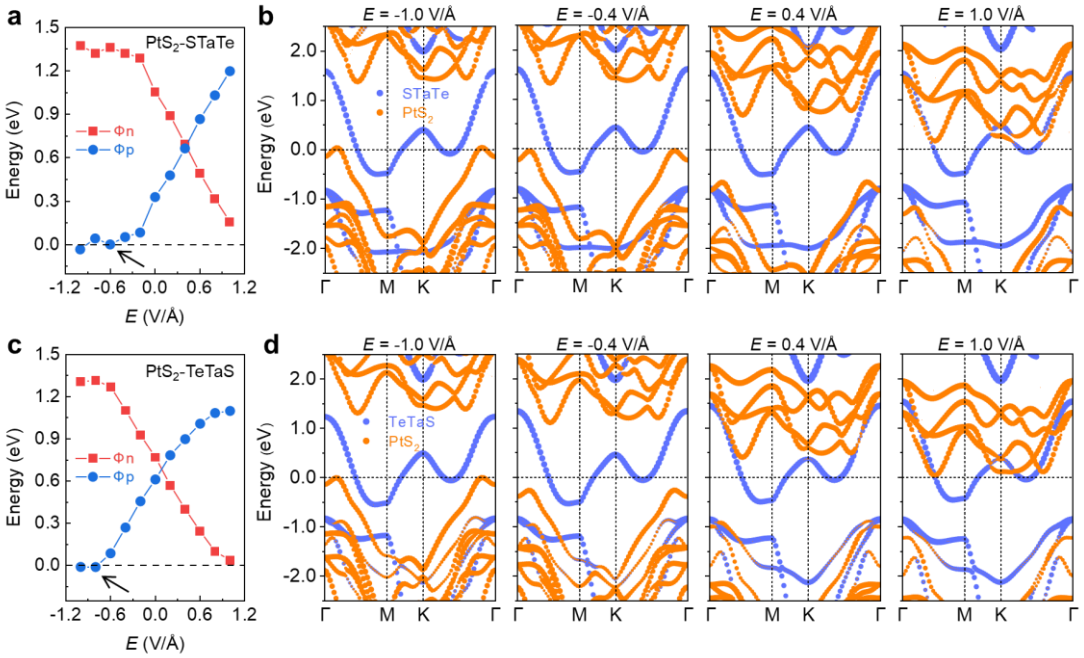

Fig. S10 Evolutions of SBH and the projected band structures under different external electric fields for (a) and (b) vdW 2L PtS_2-STaTe, (c) and (d) vdW 2L PtS_2-TeTaS heterostructures, respectively. The arrows in (a) and (c) indicates the transition from Schottky contact to Ohmic contact. Orange and blue colors in band structures represent the contributions from PtS_2 and TaSTe, respectively.

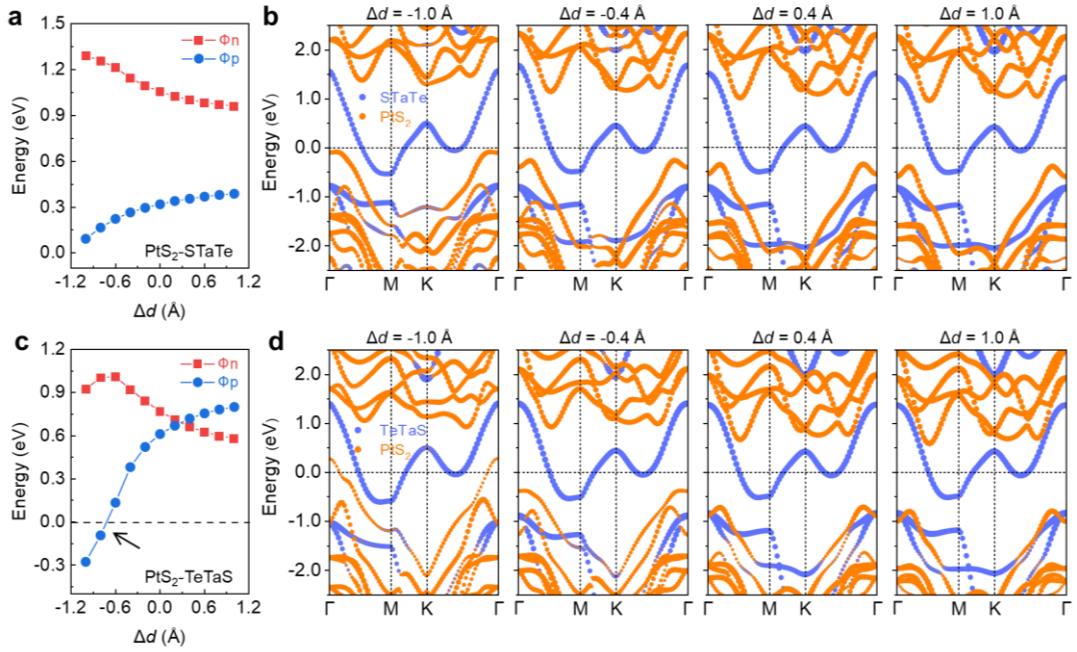

Fig. S11 Evolutions of SBH and the projected band structures under different compression and tension strains for (a) and (b) vdW 2L PtS_2-STaTe, (c) and (d) vdW 2L PtS_2-TeTaS heterostructures, respectively. The arrow in (c) indicates the transition from Schottky contact to Ohmic contact. Orange and blue colors in band structures represent the contributions from PtS_2 and TaSTe, respectively.

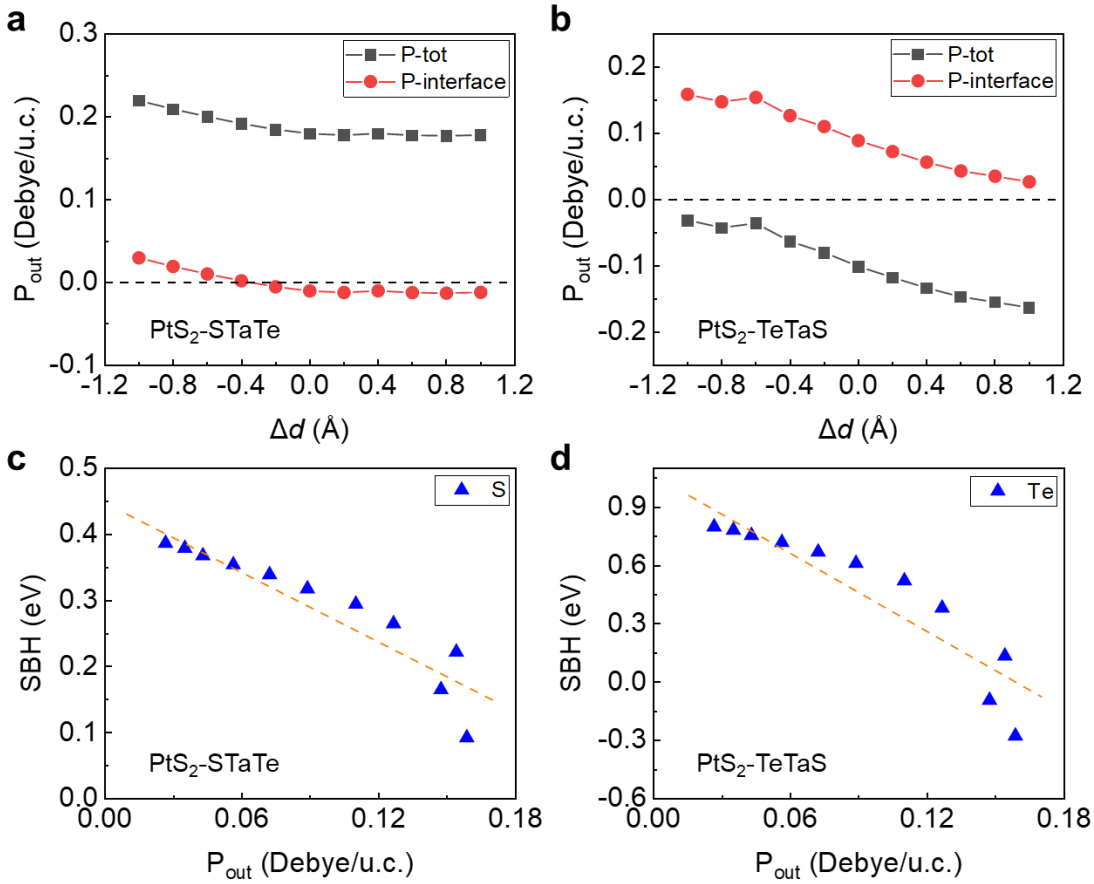

Fig. S12 (a) and (b) Out-of-plane total polarizations and interfacial polarizations versus different compression and tension strains, (c) and (d) Evolutions of SBH versus the out-of-plane interfacial polarizations for vdW 2L PtS_2-STaTe and 2L PtS_2-TeTaS heterostructures, respectively.

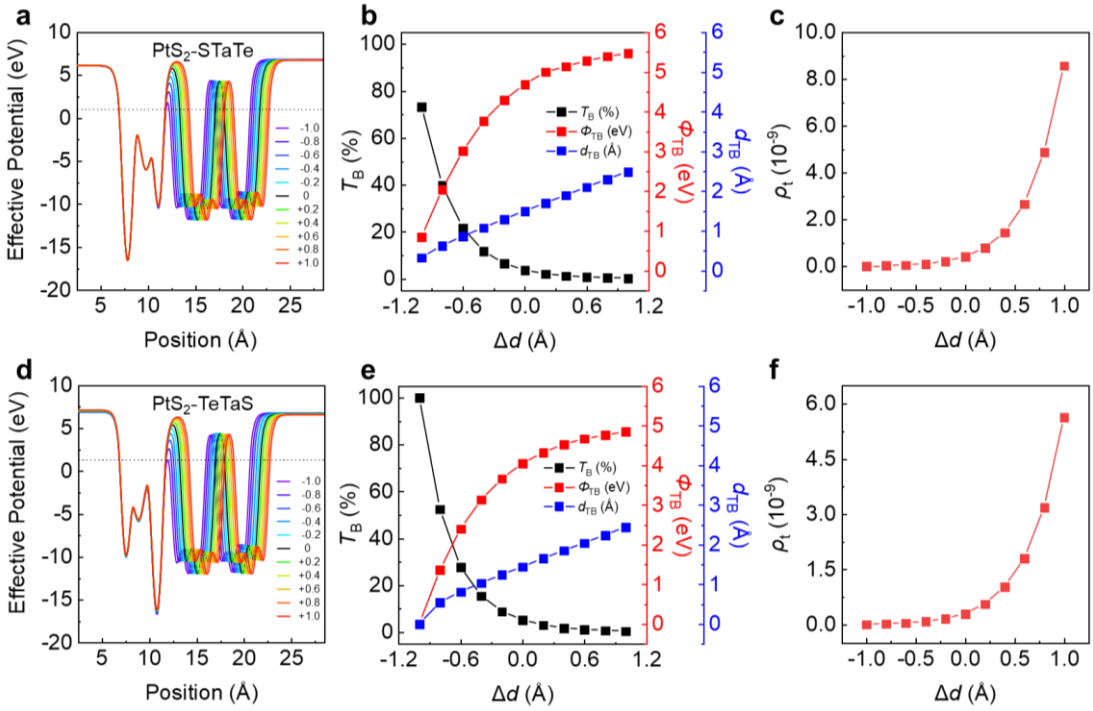

Fig. S13 (a) and (d) Out-of-plane effective potential, (b) and (e) Tunneling barrier T_B and tunneling barrier including barrier height Φ_{TB} and barrier width d_{TB}, (c) and (f) Tunneling-specific resistivity for vdW 2L PtS_2-STaTe and 2L PtS_2-TeTaS heterostructures under different compression and tension strains, respectively.

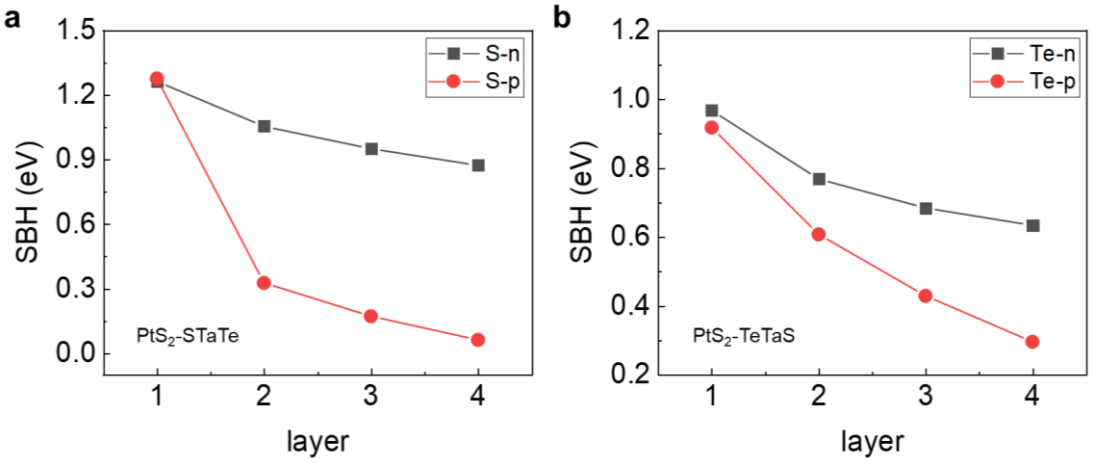

Fig. S14 Evolutions of SBH versus the layer numbers of PtS_2 for vdW (a) PtS_2-STaTe and (b) PtS_2-TeTaS heterostructures, respectively.

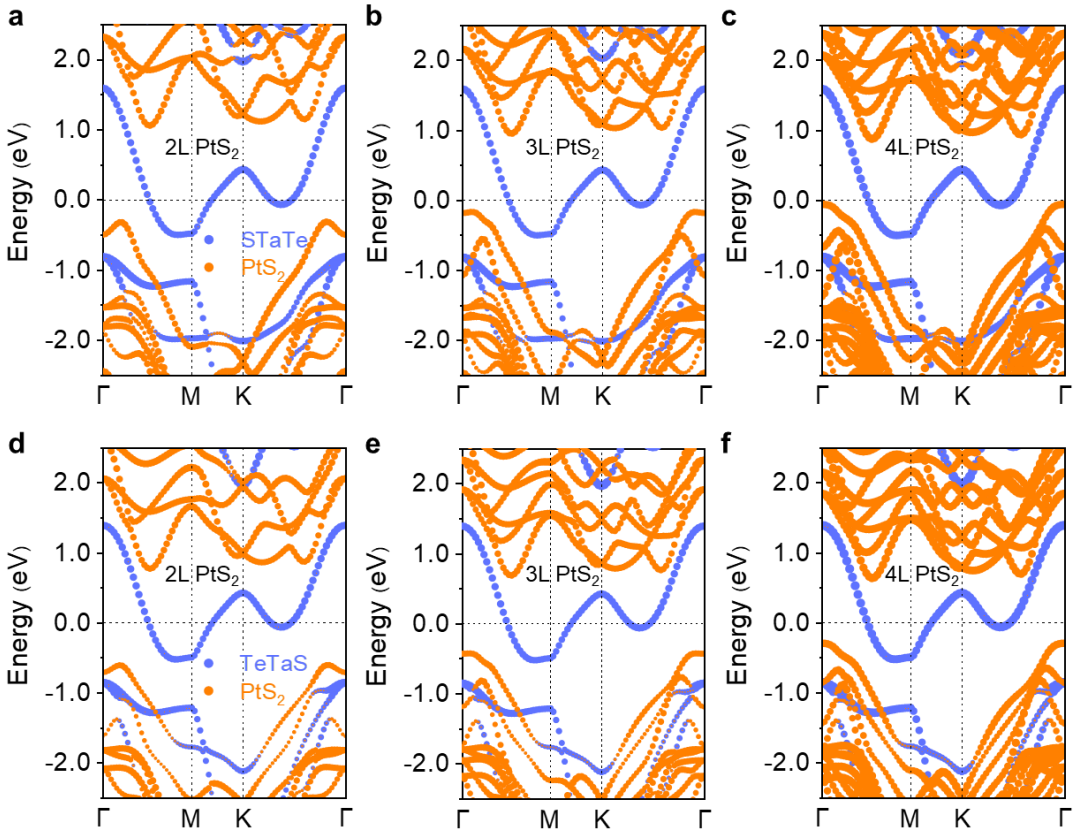

Fig. S15 Evolutions of the projected band structures versus the layer numbers of PtS_2 for vdW (a)-(c) PtS_2-STaTe, (d)-(f) PtS_2-TeTaS heterostructures, respectively. Orange and blue colors in band structures represent the contributions from PtS_2 and TaSTe, respectively.

Table S4 *n*-type and *p*-type SBHs of PtS_2-SMTe (*Φ*-S) and PtS_2-TeMS (*Φ*-Te) heterostructures. Here, M represents the transition metal elements including Hf, Zr, Ti, Nb, Cr.

(eV)	*Φ*-S-*n*	*Φ*-S-*p*	*Φ*-Te-*n*	*Φ*-Te-*p*
PtS_2-HfSTe	0.56	1.78	0.39	1.57
PtS_2-ZrSTe	0.92	1.64	0.57	1.36
PtS_2-TiSTe	0.69	1.74	0.36	1.60
PtS_2-NbSTe	1.50	0.96	1.18	0.73
PtS_2-CrSTe	1.68	0.72	1.37	0.62

Table S5 Comparison of SBH engineering method in this work with the established methods including work function engineering and interface dipole modification.

Mechanism	Tunability range (eV)	Stability	Implementation complexity	Reference
Interface dipole modification	Φn: 0.99 to 1.75 Φp: 1.02 to 1.92	Stable	Feasible	1
Interface dipole modification	Φn: 0.29 to 0.88 Φp: 0.57 to 0.67	Stable	Feasible	2
Work function engineering	Φ: 0.01 to 0.86	Stable	Feasible	3
Work function engineering	Φn: 0.00 to 1.10	Stable	Feasible	4
Work function engineering	Φn: 1.14 to 2.21	Stable	Feasible	5
Work function engineering	Φn: 0.20 to 1.12 Φp: 0.34 to 1.40	Stable	Feasible	6
Janus metal engineering	Φn: 0.97 to 1.26 Φp: 0.92 to 1.28	Stable	Feasible	Our work

References:

1. L. Peng, Y. Cui, L. Sun, J. Du, S. Wang, S. Zhang and Y. Huang, *Nanoscale Horiz.*, 2019, **4**, 480-489.

2. N. Zhao and U. Schwingenschlögl, *Nanoscale*, 2020, **12**, 11448-11454.

3. T. Shen, J.-C. Ren, X. Liu, S. Li and W. Liu, *J. Am. Chem. Soc.*, 2019, **141**, 3110-3115.

4. X. Zhang, L. Feng, S. Zhong, Y. Ye, H. Pan, P. Liu, X. Zheng, H. Li, M. Qu and X. Wang, *Sci. China Mater.*, 2023, **66**, 811-818.

5. X. Wei, M. Zhang, X. Zhang, Y. Lin, Z. Jiang and A. Du, *J. Phys. Chem. Lett.*, 2024, **15**, 3871-3883.

6. Y. Pan, J. Gu, H. Tang, X. Zhang, J. Li, B. Shi, J. Yang, H. Zhang, J. Yan, S. Liu, H. Hu, M. Wu and J. Lu, *ACS Appl. Nano Mater.*, 2019, **2**, 4717-4726.